Journal of Materials Chemistry A

PAPER

View Article Online
View Journal | View Issue

Cite this: J. Mater. Chem. A, 2014, 2, 19036

A coordinatively cross-linked polymeric network as a functional binder for high-performance silicon submicro-particle anodes in lithium-ion batteries†

Li Zhang,‡* Liya Zhang,‡ Lili Chai, Peng Xue, Weiwei Hao and Honghe Zheng*

Received 20th August 2014
Accepted 19th September 2014

DOI: 10.1039/c4ta04320k

www.rsc.org/MaterialsA

Silicon offers an extremely high theoretical specific capacity, but suffers from dramatic volume change during lithiation/delithiation processes, which typically leads to rapid anode degradation. Here we designed a facile and self-assembly strategy to construct a three-dimensional (3D) polymeric network as a promising binder for high-performance silicon submicro-particle (SiSMP) anodes through *in situ* interconnection of alginate chains by additive divalent cations. The highly cross-linked alginate network exhibits superb mechanical properties and strongly interacts with SiSMPs, which can tolerate the volume change of SiSMPs and restrict the volume expansion of the laminates to a large degree, thus effectively maintaining the mechanical and electrical integrity of the electrode and significantly improving the electrochemical performance. As a result, SiSMPs with a 3D binder network exhibit high reversible capacity, superior rate capability and much prolonged cycle life. Additionally, the 3D alginate binder was also successfully applied for the industrial submicro-silicon waste from solar cell production. With all of the advantages, the innovative way to tolerate the severe volume change by using a high-strength polymeric network may open a new approach to realize the industrial application of Si-based anodes in lithium-ion batteries.

1. Introduction

Developing rechargeable lithium-ion batteries (LIBs) with high energy density, superb rate capability and satisfactory cycle life is of great importance to meet the ever-increasing power demands of portable electronics, low-emission electrical vehicles and grid-scale energy storage systems.[1–5] In particular, materials with high lithium storage capacities are highly challenging but essential to boost the energy density and lower the cost of LIBs.[6,7] In terms of anode materials, silicon (Si) appears to be an extremely attractive candidate owing to its high theoretical specific capacity (>3500 mA h g^{-1}), low charge–discharge potential plateaus, abundance in nature and environmental benignity.[6–20] However, the widespread application of Si-based anodes in LIBs has remained a significant challenge due to its severe volume change (*ca.* 300%) associated with lithiation/delithiation processes, which results in irreversible pulverization, rapid loss of electrical contact, rearrangement and excessive growth of the solid electrolyte interphase (SEI) and therefore a drastic capacity degradation.[7–9,21–25]

To address these challenges, various strategies in architecture design and preparation technology have been put forward to overcome the large volume effect of Si by reducing the particle size,[7,10,21] depositing a micro or nano-level thick thin film[13,26,27] and dispersing active particles into an active or inactive solid matrix.[19,20,28] Among these efforts, the use of nanostructured materials to improve the lifetime of Si-based anodes has been extensively studied because of their ability to alleviate mechanical strain and prevent pulverization induced by the volume change.[7,29,30] Chemically synthesized Si nanostructures, including nanowires,[10] nanotubes,[23] nanospheres,[22] nanoporous materials[28,31] and Si–carbon (or graphene) nanocomposites,[6,17,18,25,32] have shown superior performance compared with micro-sized Si particles. However, although the pulverization issue is effectively resolved by the use of nanoscaled materials, decreasing the particle size is still not practical to entirely solve the mechanical instability issue associated with the lithium alloy because the movements of Si nanostructures and the degradation of inter-particle electrical connections can still be observed due to the inherent and repeated volume change during long-term battery cycling.[8,14,30,33,34]

Recently, increasing attention has been devoted to the advancement of the electrically inactive components of battery electrodes, such as binders.[14,16,30,33–37] Traditionally, electrode binders were believed to play a sole role in holding active

College of Physics, Optoelectronics and Energy & Collaborative Innovation Center of Suzhou Nano Science and Technology, Soochow University, Suzhou, Jiangsu, 215006, P. R. China. E-mail: zhangli81@suda.edu.cn; hhzheng@suda.edu.cn

† Electronic supplementary information (ESI) available: Additional characterization (FTIR, XRD, SEM and N_2 sorption isotherms). See DOI: 10.1039/c4ta04320k

‡ These authors contributed to this work equally.

materials and conductive additives into a cohesive laminate and providing the adhesion between the laminate and the current collector. Yet, there is now recognition of the critical role of some functional binders in maintaining the mechanical and electrical integrity of high-capacity electrodes with dramatic volume change and thereby enabling them to achieve repeatable LIB operation.[14,16,30,33–39]

Considering the severe volume effect of Si, an ideal binder is expected to possess two critical functions: first, strong interactions (hydrogen bonds or covalent bonds) between the binder and the Si surface instead of weak van der Waals forces are essential to achieve a tight anchoring of the polymeric binder onto the Si surface and enable a self-healing process (*i.e.* breaking and reformation of the bonds),[14,16,33–35,37] thereby helping to maintain the conducting environment of the Si particles and accommodate the textural stresses. Second and more importantly, robust chemical interactions (covalent bonds or coordinate bonds) between the binder chains are highly required to construct a three-dimensional (3D) cross-linked network surrounding the Si particles.[16,34–36,39,40] This 3D robust network allows superb mechanical strength and high resistance to strain, which can remarkably confine the Si particles in place and tolerate the volume change, thus effectively maintaining the electrical and mechanical integrity of the electrode and improving the electrochemical performance. Recent studies have shown that synthetic and bio-derived polymers which contain carboxylic groups, such as alginate,[14] polyacrylic acid (PAA)[41,42] and carboxy-methyl cellulose (CMC),[37,43] demonstrate promising characteristics as binders for Si-based anodes due to their high modulus values and the strong hydrogen bonding effect with the hydroxylated Si surface.[14,37] However, the interactions between the binder chains are still weak physical crosslinks (van der Waals force and hydrogen bonds), therefore reasonably stable anode performance could only be achieved when Si volume changes were minimized by incomplete lithium insertion,[43] use of ultra-small particles (20–50 nm in diameter)[14,33,34] and extra-large binder content,[37,44] which lowers the resulting anode performance. Consequently, an innovative strategy to build a 3D network on the basis of above linear polymers by introducing suited chemical interactions is of great importance to further improve the electrochemical performance of Si-based anodes. Choi *et al.* proposed a novel approach to introduce covalent ester bonds between PAA and CMC chains through a thermal condensation reaction at 150 °C and form a cross-linked binder network, which effectively improved the electrochemical performance of the Si nanoparticle (SiNP) based anode.[34] Very recently, Liu *et al.* proposed a calcium cross-linked alginate hydrogel as the novel binder for the high-performance Si–C composite anode,[40] however, the mass ratio between $CaCl_2$ and alginate residues is only 1%, revealing a very low cross-linking degree. Therefore, the low mass content of Si (42.4 wt%) and the high mass content of the binder (29 wt%) were employed due to the low mechanical properties. In addition, there is no strong interaction between the binder and the carbon shell surrounding the silicon nanoparticles, which has been previously identified as one of the most critical factors affecting the stability of Si-based anodes.[14,16,37]

In this work, we design a facile and self-assembly strategy to *in situ* construct a 3D highly cross-linked alginate network as a functional binder for high-performance silicon submicro-particle (SiSMP, ~200 nm in diameter) anodes. The 3D polymeric network with a high cross-linking degree can greatly enhance the mechanical properties of the SiSMP-based laminates through two ways: one by interconnecting alginate chains by a high concentration of Ca^{2+} cations through robust coordinate bonds, and the other by forming strong hydrogen bonding between the free alginate carboxylic groups and the hydroxylated Si surface. This highly cross-linked network can not only tolerate the severe volume change of Si upon deep galvanostatic cycling, but also restricts the volume expansion of the laminates. All these help to maintain the electrical and mechanical integrity and significantly improve the electrochemical performance of the Si anode. As a result, SiSMPs with a 3D binder network exhibit a high reversible capacity of 2522 mA h g^{-1} after 500 cycles with a capacity retention of 76.5% and maintain a superior capacity of 1646 mA h g^{-1} at the high current density of 20 C (84 A g^{-1}). In addition to improving performance of SiSMPs, the highly cross-linked alginate binder was first successfully applied for the industrial submicro-silicon waste from solar cell production. There is no doubt that the use of low-cost industrial submicro-silicon waste is of great significance to promote the practical application of silicon. We therefore anticipate that this innovative 3D polymeric network combining superb mechanical properties and strong interactions with Si can open a new approach to realize the industrial application of Si-based anodes in LIBs.

2. Experimental section

Materials and methods

Commercial silicon submicro-particles (SiSMPs, 99.9% purity) with an average particle size of ~200 nm were purchased from the Guangzhou Institute of Energy Conversion (GIEC, China). Industrial submicro-silicon wastes were provided by Suzhou GCL Photovoltaic Technology Co., Ltd. Alginate sodium salt (CAS no. 9005-38-3) with medium viscosity and anhydrous calcium chloride (analytical grade) were obtained from Sigma-Aldrich Co., Ltd. Super P carbon black with an average particle size of 30 nm was acquired from TIMCAL Graphite & Carbon (Switzerland) and the PVDF (KF1100) binder was obtained from Kureha, Japan.

Preparation of SiSMP electrodes

SiSMP laminates with an alginate binder of different molar fractions of Ca^{2+} ions were prepared by mixing SiSMPs, super P carbon black, and Na-alginate in a weight ratio of 70 : 15 : 15 in an adequate amount of Milli-Q water (Millipore, USA), and the total solid content (including SiSMPs, carbon additive and Na-Alg) was around 20 wt% in the mixture. Then different amounts of calcium chloride (the molar fractions between Ca^{2+} and alginate residues were set at 0, 0.05, 0.1 and 0.15, respectively) were added into the slurry. Upon adding Ca^{2+} ions, alginate chains were immediately cross-linked, resulting in a viscous gel.

The viscous gel was then stirred using a high shear dispersing emulsifier (Fluko FA25, Germany) for 30 min and immersed in Milli-Q water for 10 min to remove residual chloride ions. Subsequently, the filtered gel was cast onto a 15 μm-thick copper foil (99.99% purity) and the mass loading of SiSMPs was controlled to be around 1.0–1.1 mg cm^{-2}, followed by vacuum drying at 120 °C in a vacuum oven for 12 h. The preparation of industrial submicro-silicon waste based electrodes was accomplished through the same procedures.

Material characterization

The material morphology was observed with scanning electron microscopy using a Hitachi S-4700 operating at 15 kV accelerating voltage. The elemental and structural analysis was carried out by X-ray diffraction (PANalytical X'Pert PRO, Ni-filtered Cu-Kα radiation, the Netherlands) and Fourier transform infrared (FTIR) spectroscopy (TENSOR 27, BRUKER OPTICS, Germany). The nitrogen adsorption and desorption isotherms were collected at −196 °C in the range of relative pressures of 0.05–0.99P/P_0 using a TriStar II 3020 surface area and porosity measurement system (Micromeritics Instrument Co.) and used for measurements of the specific surface area (SSA) and pore size distribution in the 1.7–60 nm range. After drying the powder under vacuum at 80 °C for 12 h, 200 mg of the SiSMP sample was degassed under N_2 (99.99% purity) flow at 300 °C for 3 h before weighing and gas sorption measurements. The SSA was calculated from the Brunauer–Emmett–Teller plot. Adhesion tests of SiSMP-alginate laminates were performed on a high-precision force measurement system (TY8000, Tianyuan™, China). The Cu side of SiSMP-alginate electrodes (2 cm × 3 cm) was fixed vertically to the bottom sample holder. The adhesive side of a 3 M tape was firmly applied onto the electrode laminate side. By pulling the tape at a constant displacement rate of 200 μm s^{-1}, a layer of the SiSMP-alginate laminate was peeled off and adhered to the moving tape. The force required to peel off the laminate was recorded as an indication of the sum of interactions between the alginate chains and hydrogen bonding forces between the hydroxylated Si surface and free alginate carboxylic moieties. The compatibility of the binder with the electrolyte solvent was examined by the swelling test. Binder sheets were prepared by using solution/gel-cast samples and the solvent was removed in a vacuum oven at 90 °C. Binder sheets were then immersed in the electrolyte consisting of 1 M $LiPF_6$ salt in a mixture of ethylene carbonate (EC), dimethyl carbonate (DMC) and ethyl methyl carbonate (EMC) (1 : 1 : 1 by volume). Weight measurements were made by blotting the samples dry and immediately weighing them. The swelling ratio was defined as the weight ratio of the amount of solvent absorbed to the dry weight of the tested binder sheets.

Electrochemical characterization

The electrochemical performance was measured with CR2032-type coin cells assembled in an argon-filled glove box. The as-prepared SiSMP laminates were punched into circular discs of *ca.* 1.33 cm^2. Lithium foil was used as the counter electrode. The electrolyte used in electrochemical cells was composed of 1 M $LiPF_6$ salt in a mixture of ethylene carbonate (EC), dimethyl carbonate (DMC) and ethyl methyl carbonate (EMC) (1 : 1 : 1 by volume, Novolyte Technologies). Galvanostatic charge–discharge cycling was performed on a Maccor S4000 (Maccor Instruments, USA) between 10 mV and 1 V. The *C* rates were calculated according to the theoretical capacity of Si (4200 mA h g^{-1}). All the electrodes were discharged (lithiation) and charged (delithiation) at the same rate till 2 C (8.4 A g^{-1}), and then the discharge rates were kept at 2 C and the charge rates varied from 5 C to 20 C. Cyclic voltammetry in the potential window of 10 mV and 2 V at a rate of 0.05 mV s^{-1} was performed on an Autolab potentiostat (Autolab Instruments, Switzerland). Electrochemical impedance spectroscopy (EIS) was carried out by applying an alternating voltage of 5 mV over the frequency ranging from 10^{-2} to 10^5 Hz. All impedance measurements were carried out at 60% DOD (depth of discharge) after different electrochemical cycles.

3. Results and discussion

Alginate (commonly in the sodium salt form) is a natural exopolysaccharide extracted from brown seaweeds and some bacteria.[14] Chemically, alginates are linear copolymers of (1 → 4)-linked β-D-mannuroate (M) and α-L-guluronate (G) residues, with a varying G/M ratio. These residues are arranged in a blockwise pattern with homogeneous blocks (G–G and M–M) interspersed with M–G alternating blocks (Fig. 1a).[14,45,46] When some divalent transition metal cations such as Ca^{2+} are introduced into the aqueous solution of alginate, the divalent cations are able to coordinate within the cavities created by a pair of G–G blocks from two alginate chains through four strong coordination bonds and thus set up a bridge between adjacent alginate chains (Fig. 1a, region I).[45,46] A 3D cross-linked polymeric network architecture is therefore obtained and this brings about a sol–gel phase transition depending on the molar fraction of the bridge cations (Fig. 1b). Fourier transform infrared (FTIR) spectroscopy studies further confirm the strong interaction between the alginate chains and Ca^{2+} cations (Fig. S1†). The FTIR spectrum of Na-alginate shows the bands around 3450, 1612, 1415 and 1032 cm^{-1}, ascribed to the stretching of –OH, $–COO^-$ (asymmetric), $–COO^-$ (symmetric) and C–O–C (asymmetric), respectively.[14,40,45,46] After cross-linking by Ca^{2+} ions, the peak width of the above four peaks markedly broadens and the relative intensity significantly decreases when compared to pure Na–alginate, indicating the existence of strong coordination bonds between Ca^{2+} ions and alginate chains.

Normally, for the commonly used sodium alginate aqueous solution, the mass fraction of alginate is controlled less than 5% to ensure good fluidity. Therefore, the Alg-Ca gelatin usually consists of more than 95% water inside even a small amount of calcium chloride is introduced, revealing that a large percent of free space can be utilized for solid materials' storage.[14,37,45,46] When the Alg-Ca gelatin is mixed with Si particles to form homogenous slurry, Si particles are well dispersed into the polymeric network consisting of highly cross-linked alginate chains (Fig. 1c). This special 3D network offers excellent

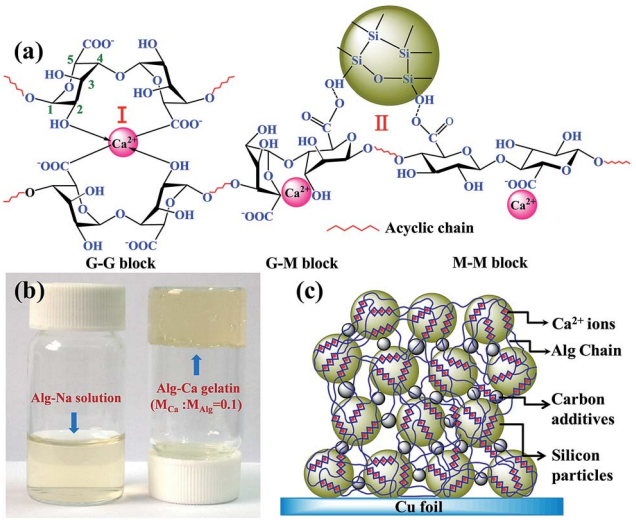

Fig. 1 (a) Schematic representation of robust coordinate bonds between alginate chains and calcium cations (region I) and strong hydrogen bonding between the hydroxylated Si surface and free alginate carboxylic groups (region II). (b) Digital images of viscous sodium alginate solution and elastic calcium cross-linked alginate gelatin. (c) Representative architecture of anodes consisting of Si particles, 3D highly cross-linked alginate network and embedded carbon additives.

mechanical strength due to the strong chemical interactions between alginate chains. The binder can therefore act as a robust matrix accommodating the severe volume change of Si particles and maintain the electrical and mechanical integrity of the electrode during long-term cycles. Moreover, the strong hydrogen bonding between the hydroxylated Si surface and free alginate carboxylic groups (Fig. 1a, region II),[14,16,34,35,37] which has been previously identified as one of the most critical factors affecting the stability of Si-based anodes, is beneficial to the tight anchoring of the alginate binder onto the Si surface and enables a self-healing process (*i.e.* breaking and reformation of the bonds),[14,16,37] thereby further enhancing the mechanical properties of the whole laminate and helping to maintain the conducting environment of the Si particles.

Scanning electron microscopy (SEM) images show that the majority of commercial SiSMPs used in this study are elliptical or spherical in shape with diameter in the range of 110 to 300 nm (Fig. S2a†). It can also be seen that most SiSMPs agglomerate into peanut-like structures with a bigger axial length up to 650 nm (Fig. S2b†). Fig. S3a† shows the X-ray diffraction pattern of the SiSMPs. All diffraction peaks in the spectrum can be clearly indexed to the cubic Si phase (JCPDS Card no. 01-0787). The sharp diffraction peaks imply that SiSMPs are well crystallized. No noticeable diffraction peaks associated with impurities are detected, reflecting the high purity of the SiSMPs. The nitrogen gas sorption isotherms of SiSMPs are presented in Fig. S3b,† and the specific surface area of SiSMPs calculated using the Brunauer–Emmett–Teller equation is *ca.* 14 $m^2\ g^{-1}$, which is significantly lower than 50–100 $m^2\ g^{-1}$ found in SiNPs.[14,33] Assuming that the density of SiSMPs is 2.34 $g\ cm^{-3}$, the average particle size is calculated to be ~200 nm, which is in accordance with what we observed in SEM studies.

SEM images of Si electrodes prepared with the calcium cross-linked alginate network are presented in Fig. 2a–h, in which the mass ratio between SiSMPs, conductive additive and alginate was kept at 70 : 15 : 15. Fig. S4† presents an example of a uniformly coated electrode film (7 cm × 23 cm), suggesting good potential for mass production. The obtained electrode is very smooth and uniform, and mass deviation of the coated materials is only ±0.03 mg cm^{-2} in different parts of the electrode. In addition, the coated film has a strong adhesion to the copper foil. No materials peel off during the subsequent operations in which the electrode is bended and folded repeatedly. To adjust the cross-linking degree of the binder, the mole fractions between Ca^{2+} and alginate residues were kept at 0, 0.05, 0.1 and 0.15, respectively. The as-prepared electrodes produced from the above four different molar fractions are referred to as Si-Alg (Fig. 2a and b), Si-Alg-Ca-0.05 (Fig. 2c and d), Si-Alg-Ca-0.1 (Fig. 2e and f) and Si-Alg-Ca-0.15 (Fig. 2g and h), respectively. As shown in Fig. 2, all the electrodes exhibit a similar porous architecture with randomly distributed pores (50–300 nm) between the SiSMPs. With the increasing molar fraction of calcium, it can be seen that the SiSMPs' surface becomes more and more rough. This can be associated with the

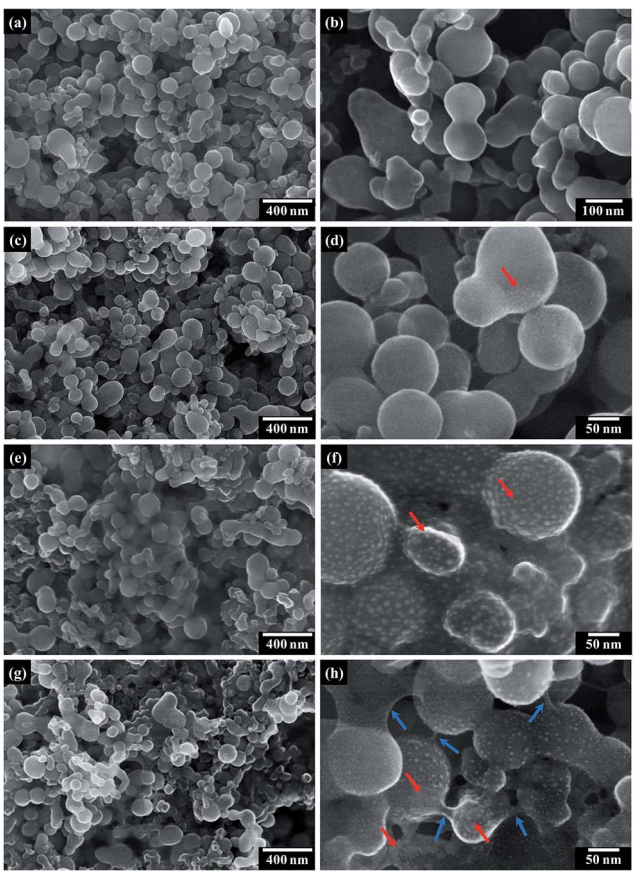

Fig. 2 SEM images of the SiSMP laminates with the alginate binder of different molar fractions of Ca^{2+} ions: (a) and (b) 0, (c) and (d) 0.05, (e) and (f) 0.1, and (g) and (h) 0.15.

increasing contraction stress within the 3D alginate network anchored on SiSMPs arising from the calcium bridge. When the alginate chains are cross-linked by more Ca^{2+} cations, the increasing retractile force leads to the formation of highly dispersed "knots" (Fig. 2f, red arrows) and aggregated "clusters" (Fig. 2h, red arrows) throughout the binder network. In particular, when the mole fraction between Ca^{2+} and alginate residues reaches 0.15, binder "bridges" emerge between the adjacent SiSMPs (the blue arrows in Fig. 2h), indicating that the cross-linking degree of the alginate chains is further enhanced.

To quantitatively evaluate and compare the mechanical properties of the SiSMP-alginate laminates with a 3D alginate network of different cross-linking degrees, adhesion tests were conducted according to a widely adopted peeling procedure (Fig. 3a).[16,33,34,40] As a reference, the peeling test result of the laminate using the poly(vinylidene fluoride) binder (Si-PVDF) is also provided. According to the force–displacement curves presented in Fig. 3b, the Si-PVDF laminate shows the lowest initial peeling force (*ca.* 2.09 N). The Si-Alg laminate exhibits higher mechanical properties than those of Si-PVDF and the initial peeling force increases to *ca.* 7.95 N. After cross-linking with Ca^{2+} cations, the mechanical properties of SiSMP-alginate laminates are significantly improved. In particular, when the mole fraction between Ca^{2+} and alginate residues reaches 0.15, the Si-Alg-Ca-0.15 laminate exhibits 14.7 and 3.85 times higher mechanical strength (*ca.* 30.6 N) than that of Si-PVDF and Si-Alg laminates, respectively. As mentioned above, the adhesion force of SiSMP-alginate laminates mainly comes from two aspects: interactions between the alginate chains and hydrogen bonding between the hydroxylated Si surface and free alginate carboxylic groups.[14,37] The adhesion test clearly indicates that the robust coordinate bonds between alginate chains contribute to the mechanical strength after cross-linking with Ca^{2+} cations, instead of weak physical crosslinks (probably van der Waals force and hydrogen bonds) between alginate chains when no cross-linking agents were added.[45,46]

To evaluate lithium ion transportation in the alginate binders of different cross-linking degrees, the electrolyte uptake was examined by the swelling test. As shown in Fig. S5,† the total electrolyte uptake of the pure alginate sheet is about 24.9% of its final weight. After cross-linking by Ca^{2+} ions, the electrolyte uptake of the Alg-Ca-0.05 and Alg-Ca-0.15 sheets increases to 26.1 and 28.3% of the final swelling weight, respectively. In addition, the Alg-Ca-0.05 and Alg-Ca-0.15 sheets show a faster wetting rate compared to that of the pure alginate sheet. The enhanced electrolyte uptake and wetting rate of the calcium cross-linked alginate sheets can be mainly attributed to the 3D network structure, which allows fast electrolyte impregnation and therefore facile Li-ion transportation through the polymer binder to the active materials.

Coin cells with lithium metal as both reference and counter electrodes were employed to investigate the electrochemical performance of SiSMP electrodes with the 3D alginate network of different cross-linking degrees. In particular, a high ratio of SiSMPs to super P carbon black (70 : 15) and a small amount of alginate binder (15 wt%) were applied for our tests in contrast to prior studies.[14,34,37] The first discharge–charge profiles in a potential range of 0.01–1 V (*vs.* Li/Li^+) at 0.05 C and cyclic voltammetry (CV) curves at a scan rate of 50 $\mu V\ s^{-1}$ of SiSMP-alginate electrodes are presented in Fig. 4a and b, respectively. All four electrodes exhibit similar lithiation/delithiation behaviour in the initial cycles. As shown in Fig. 4a, the first discharge processes mainly occur at a low voltage plateau around 0.1 V corresponding to a two-phase region where lithiated amorphous silicon (α-Li_xSi) is formed.[9] A sloping region existing between 1.0 V and 0.4 V can be ascribed to the formation of a solid electrolyte interfaces (SEI) layer at the SiSMP/electrolyte interface.[9–11,47–49] During the first charge processes, two sloping plateaus represent the two-step phase transition of α-Li_xSi into amorphous silicon (α-Si),[9,25] which are in good accordance with the two anodic peaks located at 0.32 and 0.49 V during the first positive scans (delithiation) shown in Fig. 4b.[9,11,13,49] During the second negative scans (lithiation) in Fig. 4b, two cathodic peaks appear at 0.22 V and 0.03 V, suggesting the two-step phase transition of α-Si into α-Li_xSi.[9,12,13,49] The reversible capacity for the four different Si anodes is obtained to be around 3500 mA h g^{-1}, which is not significantly affected by the content of Ca^{2+} in the binder. Nevertheless, Coulombic efficiencies of 86.1, 85.9, 83.2, and 80.2% are obtained with increasing Ca^{2+} molar fraction from 0 to 0.15. The

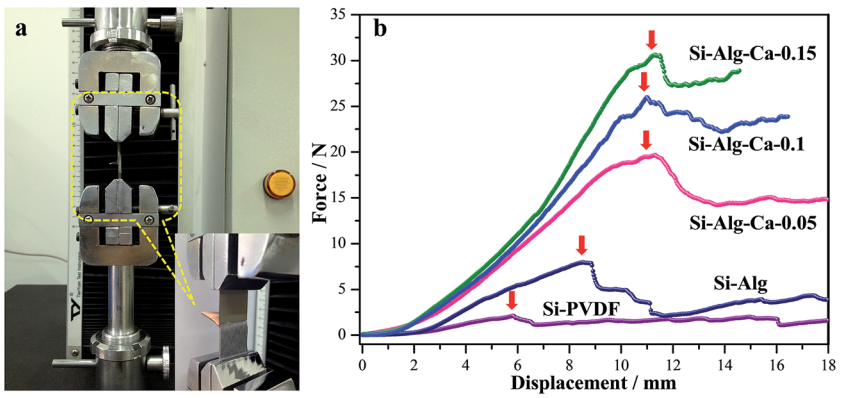

Fig. 3 Peeling tests for SiSMP-alginate laminates with the 3D alginate network of different cross-linking degrees: (a) a digital photograph of the adhesion test setup. (b) Force–displacement curves of the Si-PVDF, Si-Alg, Si-Alg-Ca-0.05, Si-Alg-Ca-0.1 and Si-Alg-Ca-0.15 laminates.

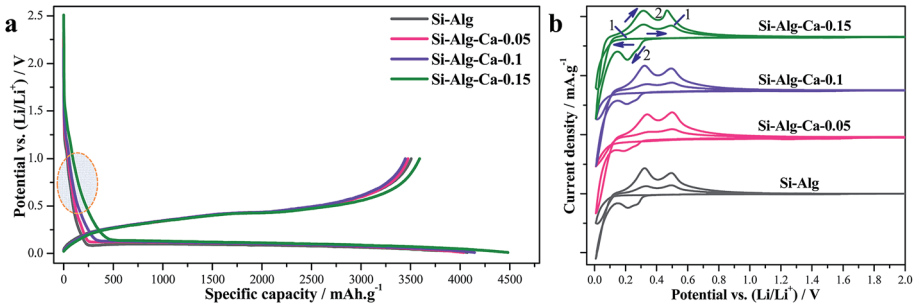

Fig. 4 (a) First galvanostatic discharge–charge profiles in a potential range of 0.01–1 V (*vs.* Li/Li^+) at 0.05 C and (b) cyclic voltammetry curves at a scan rate of 50 μV s^{-1} of the SiSMP-alginate laminates with the 3D alginate network of different cross-linking degrees.

decrease of *ca.* 6% of the first Coulombic efficiencies may be attributed to the difference in the SEI formation processes (Fig. 4a, orange circle). Previous studies have shown that the alginate binders can tightly anchor onto the Si surface by forming strong hydrogen bonds (RCOO···HOSi).[14,33,37] To a certain extent, this may prevent the access of the electrolyte to the Si-binder boundary and reduce the decomposition reaction of electrolyte components.[14] When the alginate chains are crosslinked by Ca^{2+} cations, the formation of highly dispersed "knots" or aggregated "clusters" (shown in Fig. 2) contributes to an increase of the exposed Si surface and thus brings about a certain decrease of the first Coulombic efficiency.

Electrochemical cycling performance of the SiSMP-alginate electrodes was evaluated using deep charge–discharge galvanostatic cycling from 1.0 to 0.01 V *vs.* Li/Li^+ (Fig. 5a). As a reference, the cycling performance of the electrode using the PVDF binder (Si-PVDF) is also provided. As shown in Fig. 5a, upon deep galvanostatic cycling at a current of 0.42 A g^{-1} (0.1 C), the reversible capacity of the Si-Alg electrode decreased from 2926.6 to 632.1 mA h g^{-1} after 200 cycles, exhibiting a drastic capacity loss of ~78.4%. Although this is in stark contrast to the Si-PVDF electrode, whose reversible capacity rapidly dropped to zero in less than 15 cycles, the electrode with a pure alginate binder obviously cannot endure the repeated mechanical stress aroused from the volume change of SiSMPs during long-term cycles. By contrast, with increasing Ca^{2+} molar fraction from 0.05 to 0.15, a significant improvement of long-term cycling stability is obtained. As seen in Fig. 5a, after 200 cycles, Si-Alg-Ca-0.05, Si-Alg-Ca-0.1 and Si-Alg-Ca-0.15 electrodes retained reversible capacities of 1857, 2602 and 2837.5 mA h g^{-1}, respectively, corresponding to the capacity retentions of 56.5, 79.7 and 86.2%. These results are well comparable to or even better than those in previous reports obtained from different Si nano-structures and binders.[8,14,16,32–37]

Although a pure alginate binder has been adopted to boost the cycle life of the Si anode in prior studies,[14] it seems that this binder is only effective for SiNPs with an average diameter below 50 nm.[14,36] In terms of SiSMPs of ~200 nm diameter, this binder is insufficient to endure the drastic volume expansion of Si during the lithiation process. After introducing calcium cations, the highly cross-linked alginate network is able to tolerate the severe volume change of SiSMPs upon deep galvanostatic cycling. It can thereby effectively maintain the electrical and mechanical integrity of the electrode and improve the long-term cycling performance. The smaller volume change of the Si anode with the new 3D binder can be further confirmed by measuring the thickness variation (also the volume change) of different SiSMP-alginate laminates upon first lithium insertion and extraction.[34] As shown in Fig. 5b, the Si-Alg-Ca-0.15 electrode exhibits a thickness growth of ~3 and 68.4% after the SEI formation and full lithiation processes, respectively. When it is fully delithiated, the thickness growth is ~4.5%. For the Si-Alg electrode, a much higher thickness growth of 136.4 and 39.5% in the fully lithiated and delithiated states (inset of Fig. 5b) reveals a larger irreversible volume change of the laminate. These results again indicate that the 3D alginate binder is able to tolerate the volume change of SiSMPs and restrict the volume expansion of the laminates to a large degree during electrochemical cycles. Additionally, SEM images of the Si-Alg-Ca-0.15 electrode after 200 cycles are presented in Fig. 5c–f. It is clearly seen that the morphology of the whole electrode is well preserved, and only slight cracks can be observed (the red arrow in Fig. 5c). Fig. 5d demonstrates that these cracks are 20–30 μm in length and 5–8 μm in width. Fig. 5e and f further indicate that the size of the Si particle and the porous architecture of the laminate are well preserved. Even the alginate "knots" (Fig. 5f) on the SiSMP surface can still be observed in some regions (red circle). These results clearly demonstrate that the 3D cross-linked alginate binder can maintain the electrical and mechanical integrity of SiSMP-based anodes upon deep galvanostatic cycling.

Fig. 6 provides the plots of reversible capacity and Coulombic efficiency *versus* cycle number for the Si-Alg-Ca-0.15 electrode up to 500 cycles. The electrode retains a reversible capacity of 2521.5 mA h g^{-1} with a capacity retention of 76.5%. Compared to the capacity loss of 13.8% in the initial 200 cycles (Fig. 5a), the average capacity fading rate decreases from 0.069 to 0.032% per cycle in the latter 300 cycles. This decreasing capacity fade tendency may be attributed to the increase of Coulombic efficiency of the electrode. As Fig. 6 demonstrates, the Coulombic efficiency is in a range of 98.5–99.2% in the first 200 cycles and then approaches 99.8% in the subsequent 300 cycles. Taking the severe volume change of SiSMPs during electrochemical processes into consideration, the occurrence of SEI fractures is unavoidable and this causes continuous decomposition of electrolyte components on the freshly

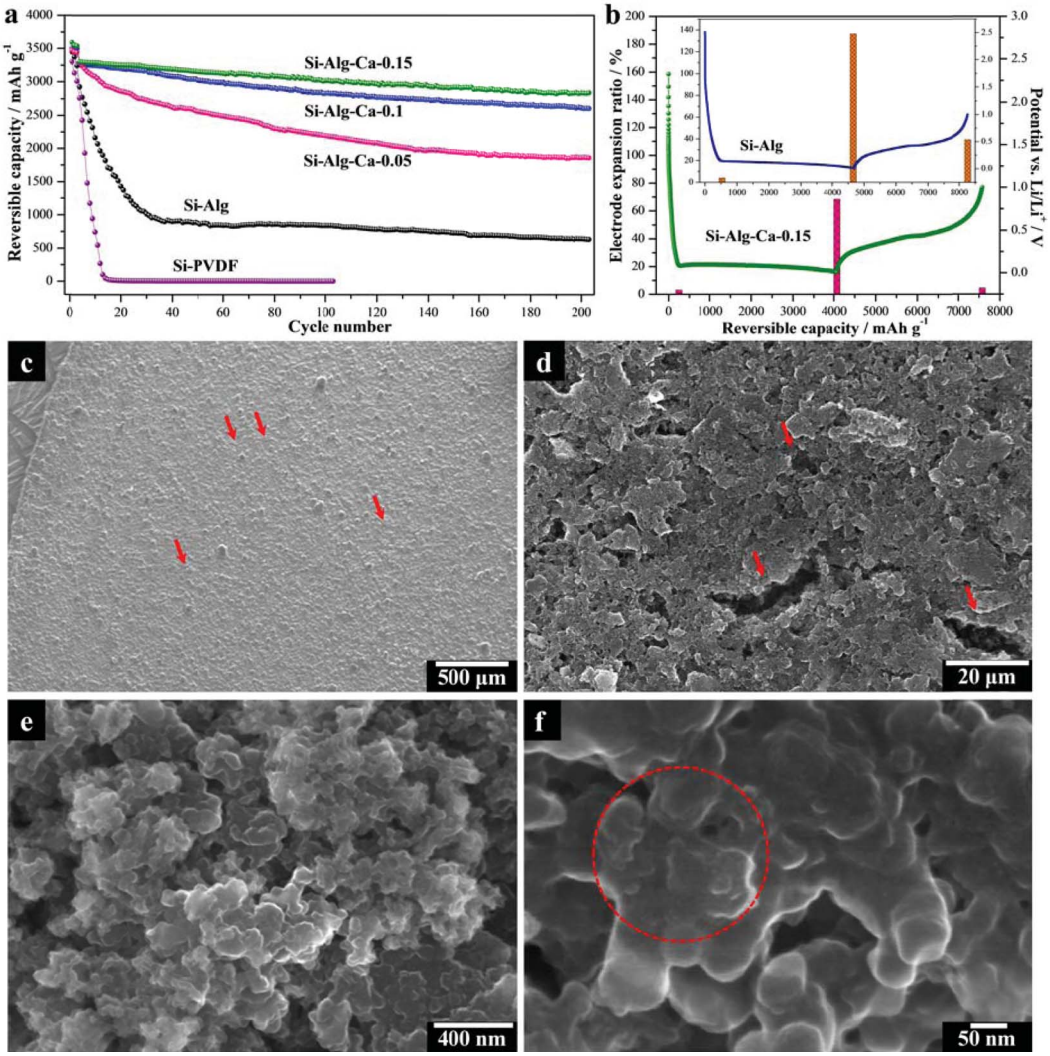

Fig. 5 (a) Plots of reversible charge capacity *versus* cycle number for the Si-PVDF electrode and SiSMP-alginate laminates with the 3D alginate network of different cross-linking degrees. (b) First galvanostatic discharge–charge profiles and thickness variation bar diagrams of the Si-Alg-Ca-0.15 electrode and the Si-Alg electrode (the inset). (c)–(f) SEM images of the Si-Alg-Ca-0.15 electrode after 200 electrochemical cycles with different magnifications.

exposed Si surface. The damage and rearrangement of the SEI layer may last for more than a hundred cycles until a stable passivating film is achieved, and thereafter the Coulombic efficiency gradually approaches 100%. To meet the requirement for commercial LIBs, further work needs to be carried out to realize *ca.* 100% Coulombic efficiency during the long-term cycling process.

It is worth noting that the mass loading of SiSMPs in this work is around 1.0–1.1 mg cm^{-2}, which is comparable or even higher than that reported in the state-of-art research studies.[14,33,34,36,37] However, we noticed that when the mass loading of SiSMPs was increased to a higher value, *e.g.*, 4.0 mg cm^{-2}, the electrodes showed a noticeably worse cycling performance. As shown in Fig. S6,† the reversible capacity of the Si-Alg-Ca-0.15 ($Si_{loading}$ = 4 mg cm^{-2}) electrode at 0.05 C is *ca.* 3451 mA h g^{-1}, which is slightly lower that of the Si-Alg-Ca-0.15 ($Si_{loading}$ = 1.1 mg cm^{-2}) electrode. After 300 cycles at 0.1 C, the Si-Alg-Ca-0.15 ($Si_{loading}$ = 4 mg cm^{-2}) electrode retained a reversible capacity of 1678 mA h g^{-1}, corresponding to a capacity retention of 54.1%. Although this is still in stark

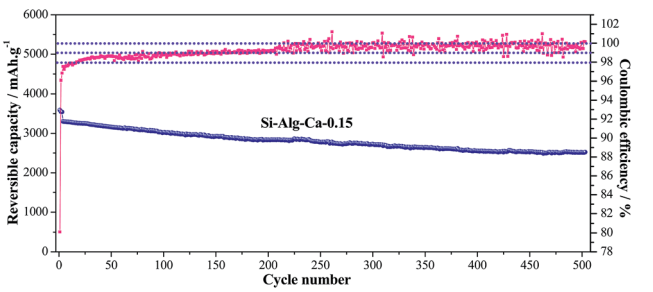

Fig. 6 Plots of reversible capacity and Coulombic efficiency *versus* cycle number for the Si-Alg-Ca-0.15 electrode up to 500 cycles.

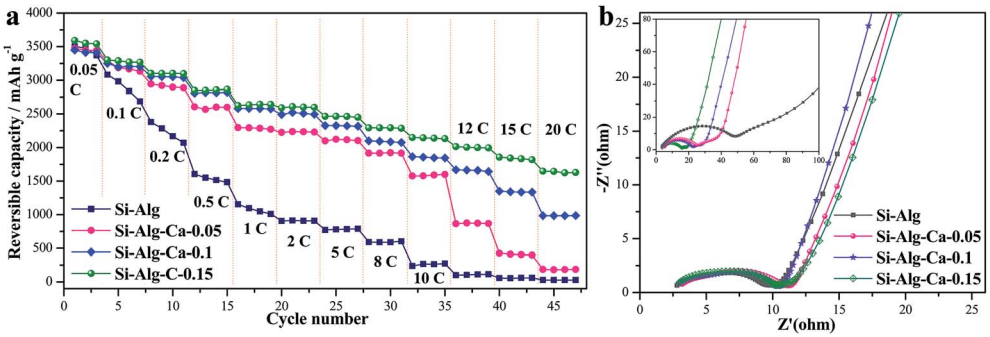

Fig. 7 (a) Rate capabilities of SiSMP-alginate laminates with the 3D alginate network of different cross-linking degrees. (b) Nyquist plots of the SiSMP-alginate laminates with the 3D alginate network of different cross-linking degrees after the formation cycles and rate capability tests (the inset).

contrast to the Si-Alg ($Si_{loading} = 1.1$ mg cm^{-2}) electrode, whose capacity retention rapidly drops to 21.6% within 200 cycles, the cycling performance of the higher loaded Si electrode needs to be further improved to achieve the commercial application of the silicon anode with a mass loading of 10–18 mg cm^{-2}. Therefore, further intensive studies are being carried out in our lab to reach this target.

Rate capabilities of the SiSMP-based anodes with alginate of different calcium molar fractions were also investigated at higher current densities. As shown in Fig. 7a, reversible capacities of the Si-Alg electrode at 0.5 C, 1 C, 5 C and 10 C are obtained to be 1483.5, 1009.8, 788.7 and 273.5 mA h g^{-1}, respectively, corresponding to ~48.6, 33.1, 25.8 and 9% of that obtained at 0.05 C (0.21 A g^{-1}). By contrast, Si-Alg-Ca-0.05, Si-Alg-Ca-0.1 and Si-Alg-Ca-0.15 electrodes exhibit significantly higher rate capabilities, especially for the Si-Alg-Ca-0.15 electrode, which works well up to 20 C and retains a reversible capacity of 1646 mA h g^{-1}, corresponding to 46.5% of that obtained at 0.05 C. The significant enhancement of rate performance of the SiSMPs by using a 3D cross-linked alginate binder should be attributed to the high mechanical properties of the binder. The binder is able to maintain the electrical and mechanical integrity of the electrode laminate upon deep galvanostatic cycling. This can be further confirmed by the electrochemical impedance spectroscopy (EIS) measurements after the formation cycles and rate capability tests (Fig. 7b). After the formation cycles, all spectra are composed of two overlapped semicircles in the high and medium frequency regions and a straight sloping line of the Warburg impedance in the low frequency regions. The high-frequency semicircle is related to

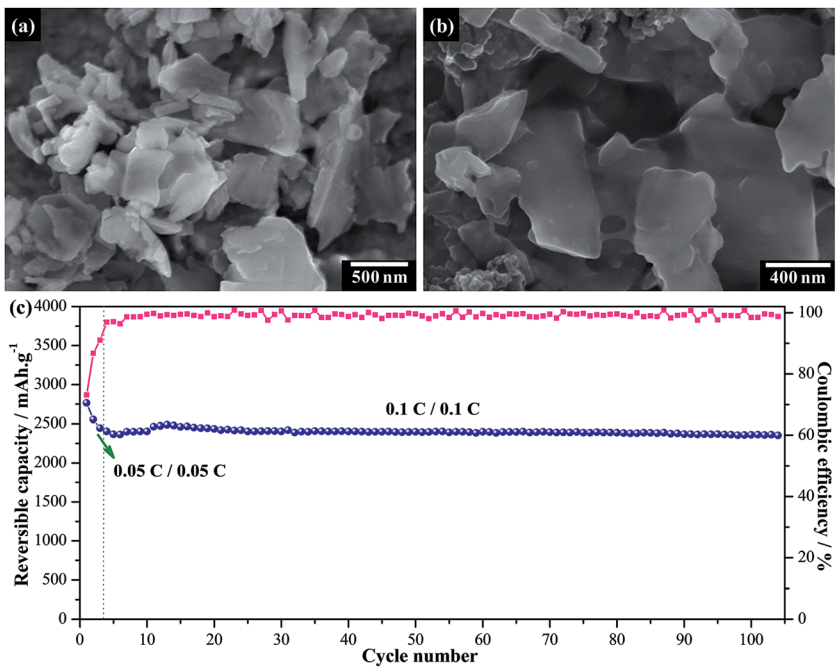

Fig. 8 (a) and (b) SEM images of the submicro-silicon wastes from solar cell production. (c) Plots of reversible capacity and Coulombic efficiency *versus* cycle number for the submicro-silicon waste based electrode up to 100 cycles.

the resistance of the passivating SEI film (R_{SEI}) and the intermediate-frequency semicircle is attributed to the charge-transfer resistance (R_{ct}).[15,25,50–54] It is clearly seen that all four electrodes show very close R_{SEI} and R_{ct} at this stage. However after the rate capability test (the inset of Fig. 7b), both the R_{SEI} and R_{ct} (especially R_{SEI}) of the Si-Alg electrode remarkably increase, revealing a considerable growth of the SEI layer. By comparison, there is only a slight increase of R_{SEI} and R_{ct} for the Si-Alg-Ca-0.15 electrode. This result indicates that the SEI film can be well stabilized by accommodating the severe volume change of Si particles using the 3D alginate network.

In addition to improving performance of commercial SiSMPs, the 3D highly cross-linked alginate binder was also applied for the industrial submicro-silicon waste from solar cell production.[55,56] These submicro-silicon particles are low-cost and easy to obtain because more than 45% of the high-purity Si turns to sub-micrometer saw powder during wafer slicing in solar cell companies.[55,56] Fig. 8a displays the SEM images of the submicro-silicon wastes, which are mainly irregular plates with a length, width and thickness of 500–1500 nm, 300–1000 nm and 150–250 nm, respectively. Fig. 8b shows the as-prepared laminate consisting of 70 wt% submicro-silicon waste, 15 wt% super P carbon black and 15 wt% alginate binder with a 0.15 molar fraction of Ca^{2+}. The electrochemical cycling performance of the submicro-silicon waste based electrode was evaluated and is displayed in Fig. 8c. After 100 cycles at 0.1 C, the electrode retains a reversible capacity of 2352 mA h g^{-1}, corresponding to the capacity retention of 97.8% of that obtained at the first cycle. The detailed investigation of the submicro-silicon waste based electrode using the 3D cross-linked polymeric network will be published in the future.

4. Conclusion

In conclusion, we have developed a facile and self-assembly strategy to *in situ* construct a 3D cross-linked polymeric network as a promising binder for high-performance SiSMP-based anodes. The highly cross-linked alginate network exhibits superb mechanical strength and strongly interacts with SiSMPs, which can tolerate the volume change of Si particles and alleviate the volume expansion of the electrodes to a large degree. In this sense, the new binder is able to effectively maintain the mechanical and electrical integrity of the electrode and significantly improve the electrochemical performance. As a result, SiSMP-based anodes with the 3D binder network exhibit high reversible capacity, superior rate capability and much prolonged cycle life. In addition to improving the performance of commercial SiSMPs, the cross-linked 3D alginate binder was also successfully applied for the industrial submicro-silicon waste from solar cell production. Considering all of the advantages, this innovative way of tolerating the severe volume effect of submicro-silicon particles by using a high strength binder network may be extended to other high-capacity electrode materials that suffer severe volume changes during long-term electrochemical cycling.

Acknowledgements

The authors are greatly indebted to the funding of the Natural Science Foundation of China (NSFC, contract no. 21203132, 21473119 and 51272168).

References

1 M. Armand and J. M. Tarascon, *Nature*, 2008, **451**, 652–657.
2 J. B. Goodenough and Y. Kim, *Chem. Mater.*, 2009, **22**, 587–603.
3 J. R. Owen, *Chem. Soc. Rev.*, 1997, **26**, 259–268.
4 A. S. Arico, P. Bruce, B. Scrosati, J. M. Tarascon and W. VanSchalkwijk, *Nat. Mater.*, 2005, **4**, 366–377.
5 M. S. Whittingham, *Chem. Rev.*, 2004, **104**, 4271–4301.
6 A. Magasinski, P. Dixon, B. Hertzberg, A. Kvit, J. Ayala and G. Yushin, *Nat. Mater.*, 2010, **9**, 353–358.
7 J. R. Szczech and S. Jin, *Energy Environ. Sci.*, 2011, **4**, 56–72.
8 H. Wu, G. Chan, J. W. Choi, I. Ryu, Y. Yao, M. T. McDowell, S. W. Lee, A. Jackson, Y. Yang, L. B. Hu and Y. Cui, *Nat. Nanotechnol.*, 2012, **7**, 309–314.
9 M. N. Obrovac and L. J. Krause, *J. Electrochem. Soc.*, 2007, **154**, A103–A108.
10 C. K. Chan, H. L. Peng, G. Liu, K. McIlwrath, X. F. Zhang, R. A. Huggins and Y. Cui, *Nat. Nanotechnol.*, 2008, **3**, 31–35.
11 J. Li and J. R. Dahn, *J. Electrochem. Soc.*, 2007, **154**, A156–A161.
12 T. D. Hatchard and J. R. Dahn, *J. Electrochem. Soc.*, 2004, **151**, A838–A842.
13 K. Evanoff, A. Magasinski, J. B. Yang and G. Yushin, *Adv. Energy Mater.*, 2011, **1**, 495–498.
14 I. Kovalenko, B. Zdyrko, A. Magasinski, B. Hertzberg, Z. Milicev, R. Burtovyy, I. Luzinov and G. Yushin, *Science*, 2011, **333**, 75–79.
15 Y. S. Hu, R. Demir-Cakan, M. M. Titirici, J. O. Muller, R. Schlogl, M. Antonietti and J. Maier, *Angew. Chem., Int. Ed.*, 2008, **47**, 1645–1649.
16 G. Liu, S. D. Xun, N. Vukmirovic, X. Y. Song, P. Olalde-Velasco, H. H. Zheng, V. S. Battaglia, L. W. Wang and W. L. Yang, *Adv. Mater.*, 2011, **23**, 4679–4683.
17 X. S. Zhou, Y. X. Yin, L. J. Wan and Y. G. Guo, *Adv. Energy Mater.*, 2012, **2**, 1086–1090.
18 X. Zhao, C. M. Hayner, M. C. Kung and H. H. Kung, *Adv. Energy Mater.*, 2011, **1**, 1079–1084.
19 R. Yi, F. Dai, M. L. Gordin, H. Sohn and D. H. Wang, *Adv. Energy Mater.*, 2013, **3**, 1507–1515.
20 R. Yi, F. Dai, M. L. Gordin, S. R. Chen and D. H. Wang, *Adv. Energy Mater.*, 2013, **3**, 295–300.
21 R. Krishnan, T. M. Lu and N. Koratkar, *Nano Lett.*, 2011, **11**, 377–384.
22 H. Ma, F. Y. Cheng, J. Chen, J. Z. Zhao, C. S. Li, Z. L. Tao and J. Liang, *Adv. Mater.*, 2007, **19**, 4067–4070.
23 M. H. Park, M. G. Kim, J. Joo, K. Kim, S. Ahn, Y. Cui and J. Cho, *Nano Lett.*, 2009, **9**, 3844–3847.
24 C. K. Chan, R. Ruffo, S. S. Hong and Y. Cui, *J. Power Sources*, 2009, **189**, 1132–1140.

25 L. Zhang, W. W. Hao, H. B. Wang, L. F. Zhang, X. M. Feng, Y. B. Zhang, W. X. Chen, H. Pang and H. H. Zheng, *J. Mater. Chem. A*, 2013, **1**, 7601–7611.
26 H. Li, X. J. Huang, L. Q. Chen, G. W. Zhou, Z. Zhang, D. P. Yu, Y. J. Mo and N. Pei, *Solid State Ionics*, 2000, **135**, 181–191.
27 F. Qu, C. L. Li, Z. M. Wang, H. P. Strunk and J. Maier, *ACS Appl. Mater. Interfaces*, 2014, **6**, 8782–8788.
28 H. Kim, B. Han, J. Choo and J. Cho, *Angew. Chem., Int. Ed.*, 2008, **47**, 10151–10154.
29 L. W. Ji, Z. Lin, M. Alcoutlabi and X. W. Zhang, *Energy Environ. Sci.*, 2011, **4**, 2682–2699.
30 M. Y. Wu, J. E. C. Sabisch, X. Y. Song, A. M. Minor, V. S. Battaglia and G. Liu, *Nano Lett.*, 2013, **13**, 5397–5402.
31 M. Y. Ge, Y. H. Lu, P. Ercius, J. P. Rong, X. Fang, M. Mecklenburg and C. W. Zhou, *Nano Lett.*, 2014, **14**, 261–268.
32 N. Liu, H. Wu, M. T. McDowell, Y. Yao, C. M. Wang and Y. Cui, *Nano Lett.*, 2012, **12**, 3315–3321.
33 M. H. Ryou, J. Kim, I. Lee, S. Kim, Y. K. Jeong, S. Hong, J. H. Ryu, T. S. Kim, J. K. Park and H. Lee, *Adv. Mater.*, 2013, **25**, 1571–1576.
34 B. Koo, H. Kim, Y. Cho, K. T. Lee, N. S. Choi and J. Cho, *Angew. Chem., Int. Ed.*, 2012, **51**, 8762–8767.
35 H. Wu, G. H. Yu, L. J. Pan, N. Liu, M. T. McDowell, Z. N. Bao and Y. Cui, *Nat. Commun.*, 2013, **4**, 1943.
36 C. Wang, H. Wu, Z. Chen, M. T. McDowell, Y. Cui and Z. N. Bao, *Nat. Chem.*, 2013, **5**, 1043–1049.
37 J. S. Bridel, T. Azais, M. Morcrette, J. M. Tarascon and D. Larcher, *Chem. Mater.*, 2010, **22**, 1229–1241.
38 M. Y. Wu, X. C. Xiao, N. Vukmirovic, S. D. Xun, P. K. Das, X. Y. Song, P. Olalde-Velasco, D. D. Wang, A. Z. Weber, L. W. Wang and G. Liu, *J. Am. Chem. Soc.*, 2013, **135**, 12048–12056.
39 Y. K. Jeong, T. W. Kwon, I. Lee, T. S. Kim, A. Coskun and J. W. Choi, *Nano Lett.*, 2014, **14**, 864–870.
40 J. Liu, Q. Zhang, Z. Y. Wu, J. H. Wu, J. T. Li, L. Huang and S. G. Sun, *Chem. Commun.*, 2014, **50**, 6386–6389.
41 S. Komaba, K. Shimomura, N. Yabuuchi, T. Ozeki, H. Yui and K. Konno, *J. Phys. Chem. C*, 2011, **115**, 13487–13495.
42 A. Magasinski, B. Zdyrko, I. Kovalenko, B. Hertzberg, R. Burtovyy, C. R. Huebner, T. F. Fuller, I. Luzinov and G. Yushin, *ACS Appl. Mater. Interfaces*, 2010, **2**, 3004–3010.
43 D. Mazouzi, B. Lestriez, L. Roue and D. Guyomard, *Electrochem. Solid-State Lett.*, 2009, **12**, A215–A218.
44 S. D. Beattie, D. Larcher, M. Morcrette, B. Simon and J. M. Tarascon, *J. Electrochem. Soc.*, 2008, **155**, A158–A163.
45 Y. P. Fang, S. Al-Assaf, G. O. Phillips, K. Nishinari, T. Funami, P. A. Williams and L. B. Li, *J. Phys. Chem. B*, 2007, **111**, 2456–2462.
46 W. Wang, X. D. Liu, Y. B. Xie, H. A. Zhang, W. T. Yu, Y. Xiong, W. Y. Xie and X. J. Ma, *J. Mater. Chem.*, 2006, **16**, 3252–3267.
47 E. L. Memarzadeh, W. P. Kalisvaart, A. Kohandehghan, B. Zahiri, C. M. B. Holt and D. Mitlin, *J. Mater. Chem.*, 2012, **22**, 6655–6668.
48 Y. H. Xu, G. P. Yin, Y. L. Ma, P. J. Zuo and X. Q. Cheng, *J. Mater. Chem.*, 2010, **20**, 3216–3220.
49 L. Baggetto, R. A. H. Niessen, F. Roozeboom and P. H. L. Notten, *Adv. Funct. Mater.*, 2008, **18**, 1057–1066.
50 C. Y. Du, C. H. Gao, G. P. Yin, M. Chen and L. Wang, *Energy Environ. Sci.*, 2011, **4**, 1037–1042.
51 P. F. Gao, J. W. Fu, J. Yang, R. G. Lv, J. L. Wang, Y. N. Nuli and X. Z. Tang, *Phys. Chem. Chem. Phys.*, 2009, **11**, 11101–11105.
52 J. C. Guo, X. L. Chen and C. S. Wang, *J. Mater. Chem.*, 2010, **20**, 5035–5040.
53 L. L. Chai, Q. T. Qu, L. F. Zhang, M. Shen, L. Zhang and H. H. Zheng, *Electrochim. Acta*, 2013, **105**, 378–383.
54 Y. Zhu and C. Wang, *J. Power Sources*, 2011, **196**, 1442–1448.
55 L. J. Fernandez, R. Ferrer, D. F. Aponte and P. Fernandez, *Sol. Energy Mater. Sol. Cells*, 2011, **95**, 1701–1706.
56 T. Y. Wang, Y. C. Lin, C. Y. Tai, R. Sivakumar, D. K. Rai and C. W. Lan, *J. Cryst. Growth*, 2008, **310**, 3403–3406.